An hourglass pattern of inter-embryo gene expression variability and of histone regulation in fly embryogenesis

Jialin Liu[1,2]*, Michael Frochaux[2,3], Vincent Gardeux[2,3], Bart Deplancke[2,3], Marc Robinson-Rechavi[1,2]*

1 Department of Ecology and Evolution, University of Lausanne, 1015 Lausanne, Switzerland

2 Swiss Institute of Bioinformatics, 1015 Lausanne, Switzerland

3 Laboratory of Systems Biology and Genetics, Institute of Bioengineering, School of Life Sciences, Ecole Polytechnique Fédérale de Lausanne (EPFL)

* corresponding authors: jialin.liu@unil.ch, marc.robinson-rechavi@unil.ch

Gene expression is in part a stochastic process [1–3], which is at odds with the need for precise expression levels in biological processes such as embryonic development. To study the tension between precision and stochasticity of gene expression during development, we quantified expression variability of single embryo transcriptomes throughout fly *Drosophila melanogaster* embryogenesis, from 150 samples over eight developmental stages. We found that expression variability follows an hourglass pattern, with lower variability at extended germband, the phylotypic stage. We explain this pattern by stronger histone modification mediated transcriptional noise control at this stage. In addition, we propose that histone modifications contribute to mutational robustness in regulatory elements, and thus to conserved expression levels. These results provide insight into the role of robustness in the phenotypic and genetic patterns of evolutionary conservation in animal development.

Phenotypes can vary even among isogenic individuals in homogenous environments, suggesting that stochastic effects contribute to phenotypic diversity [4,5]. Gene expression variability among genetically identical individuals under uniform conditions, hereafter "variability", is one of the most important stochastic processes in the mapping of genotype to phenotype. It is caused by a combination of molecular noise (stochastic biochemical effects, e.g., transcriptional burst process based transcriptional noise) and other effects (variation in cells and their environment, e.g., distribution of molecules at cell division) [2,3,6]. Precise regulation of gene expression is notably important during development [7], where it controls the exact timing and level of gene expression to make a functional embryo. However, this process inevitably has to deal with stochasticity [8].

This tension between precision and stochasticity in development raises questions, such as how expression variability is controlled or buffered during development. And whether some stages are more robust to gene expression stochasticity. This is especially interesting in relation to the “phylotypic” stage, in mid-embryonic development, and the corresponding “hourglass” model of Evo-Devo [9,10]. The phylotypic stage is characterized by conserved morphology inside a phylum, which extends to the molecular level, notably lower expression divergence between species or strains [11–15]. To answer these questions, we investigated expression variability across fly embryonic development.

We generated 288 single embryo 3' end transcriptomes using BRB-seq [16], at eight developmental stages covering the whole fly embryogenesis, with 3h intervals (Figure 1A). After quality control, 239 samples were kept (Figure S1, S2). On average, we obtained over 5 million uniquely mapped reads of protein coding genes per embryo. Based on multidimensional scaling analysis (MDS), 150 embryos follow the developmental trajectory, while there is a small cluster of 89 embryos collected at different time points mixed together (Figure 1B). The samples in this cluster appear to be unfertilized eggs (Methods and Figure S3). All further analysis was performed only on the 150 fertilized embryos.

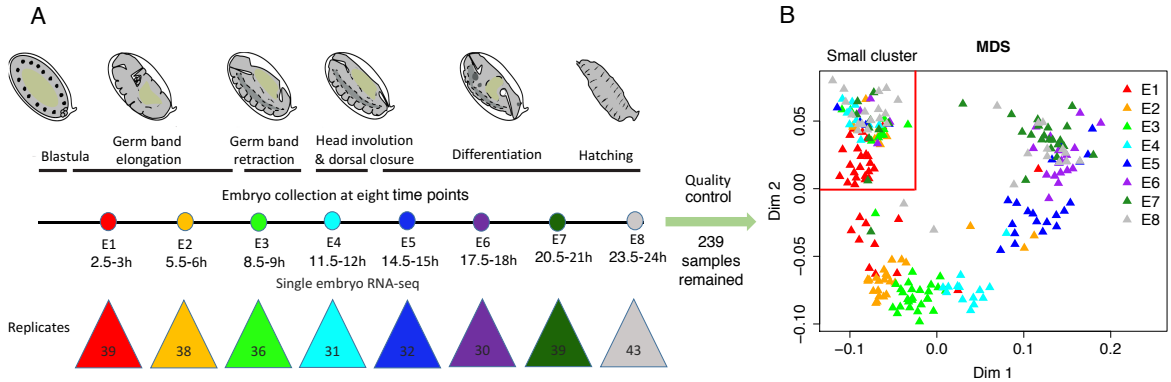

Figure 1: Studying expression variability throughout embryogenesis

A. Method outline. We performed single embryo BRB-seq[16] at eight developmental stages, indicated by different colored dots. The number of samples collected at each stage is indicated in the colored triangles. Embryo images adapted from [17] and used with permission from Springer Nature (License Number: 4547630238607) and from the authors.

B. Multidimensional scaling analysis (MDS) of 239 high quality samples. Different colors indicate different stages. The samples can be split into two groups: a small cluster in the top-left delimited by two red lines; and the remaining samples, which are organized according to embryonic stage. Only the 150 samples which follow embryonic stages were used for further analysis.

We measured expression variability as Adjusted SD, standard deviation (SD) of expression between replicates corrected for expression level (Methods and Figures S4-6). This expression variability follows an hourglass pattern overall, with a global minimum at E3 (Figure 2A), corresponding to the phylotypic stage of fly [14]. There is also a local minimum

at E6. This is consistent with the pattern of transcriptome divergence between fly and mosquito *Anopheles gambiae*, with the global minimum at E3, and a local minimum at E6 [18]. Our observations are robust to the use of different variability metrics (Figure S7), and to sampling (bootstrap analysis, Figure S8). Bootstrap results also suggest that the minimum of variability extends over E3 to E4. The embryo transcriptome is dominated by zygotic transcripts 2.5h after egg laying[19], so the high variability in E1 and E2 is not directly caused by maternal transcripts. We didn't find any significant functional enrichment for genes which follow the hourglass variability pattern. Overall, expression variability is not equally distributed throughout embryogenesis, and gene expression at the phylotypic stage appears more robust to stochastic factors than at other stages.

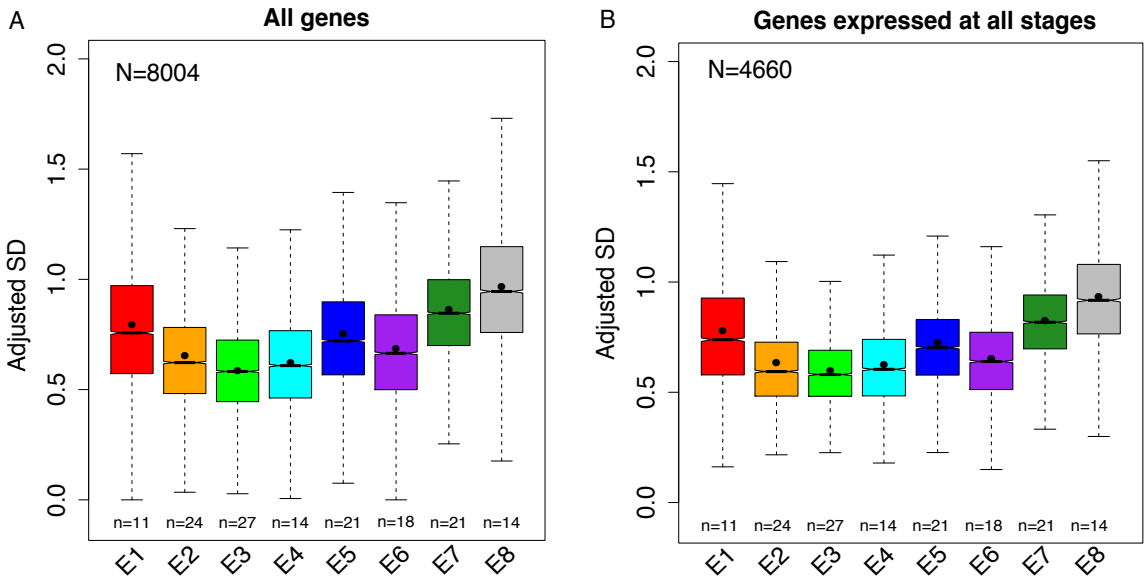

Figure 2: The phylotypic stage (E3) has lower expression variability

The number of individual samples used in each development stage is indicated below each box. The number of genes analyzed is indicated in the top-left corner of each plot. The lower and upper intervals indicated by the dashed lines ("whiskers") represent 1.5 times the interquartile range (IQR), and the box shows the lower and upper intervals of IQR together with the median. The black dot in each box indicates the mean.

A. Expression variability pattern of all genes which passed quality control. We performed pairwise Wilcoxon tests between any two stages to test the significance. The multiple test corrected p-values (Benjamini–Hochberg method) are shown in Table S1; they are all < 10^{-7}.

B. Expression variability pattern of genes expressed at all stages. We performed pairwise Wilcoxon tests between any two stages to test the significance. The multiple test corrected p-values (Benjamini–Hochberg method) are shown in Table S2; they are all < 10^{-5} except E2 vs. E4, for which p-values = 0.24.

The variation in expression variability could either be due to changes in the set of active genes, with genes differing in their intrinsic variability levels, or to genome-wide changes in the regulation of variability. To test this, we first reproduced our results restricted to the subset of genes which are expressed at all stages. Under the first explanation, we would expect to lose the hourglass variability pattern, but the pattern is maintained (Figure 2B). We performed additional tests: restricting to genes with constant expression level over development (Figure S9A); restricting to transcription factors (Figure S9B); and contrasting genes with dispersed or precise promoters (Figure S10), following Schor et al [20]. Dispersed promoters seem to be more robust to mutations, which might also translate into robustness to noise. Despite a loss of power with fewer genes, there remains an hourglass pattern of expression variability in all cases. Interestingly, the precise promoter genes have higher variability than the dispersed promoter genes except at E3, thus a strongest hourglass pattern. Overall, these results suggest that the lower variability at E3 is due to genome-wide regulation mechanisms more than to changes in the gene set.

Histone modifications can regulate transcriptional noise [21–25], notably through the modulation of transcriptional burst frequency [22–24]. For example, high levels of histone modifications can increase chromatin accessibility, leading to an increase in transcriptional burst frequency, which leads to minimizing noise. To check this role of histone modifications, we analyzed four available euchromatin histone modifications at six developmental stages [26]. For each gene, we calculated the mean modification signal (background-subtracted tag density) separately for proximal promoters and for gene bodies [23]. Higher modification signal genes tend to have lower variability for all histone modifications (Figure 3A). This supports a role in minimizing transcriptional noise, and is consistent with previous studies in yeast and mammals [22,23].

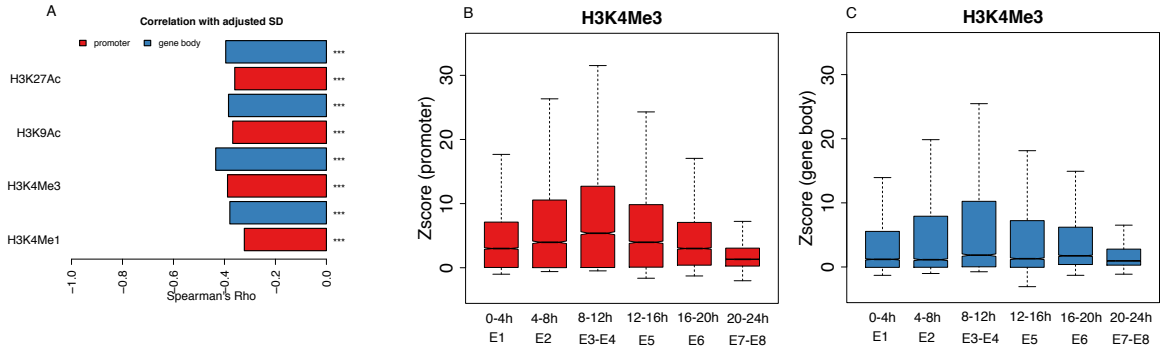

Figure 3: Histone modification signal and expression variability

Red and blue represent histone modification signals calculated on the proximal promoter (4kb around the transcription start site – TSS) and the gene body, respectively.

*A. Spearman's correlation coefficient between histone modification signal (background-subtracted tag density) and expression variability. Here, for each gene, both its variability and its histone modification signal are the mean value across stages. ***, P < 0.001; **, P < 0.01; *, P < 0.05, NS, P ≥ 0.05.*

B. Proximal promoter H3K4Me3 signal (Z score relative to intergenic signal) in different stages. Corresponding stages of our expression variability data are indicated below. The lower and upper intervals indicated by the dashed lines ("whiskers") represent 1.5 times the interquartile range (IQR), and the box shows the lower and upper intervals of IQR together with the median. We performed pairwise Wilcoxon tests between any two stages to test the significance. The multiple test corrected p-values (Benjamini–Hochberg method) are shown in Table S3; they are all $<10^{-7}$ except 4-8h vs. 12-16h, for which p-value = 0.68.

C. Gene body H3K4Me3 signal (Z score relative to intergenic signal) in different stages. Corresponding stages of our single embryo BRB-seq data are indicated below. The lower and upper intervals indicated by the dashed lines ("whiskers") represent 1.5 times the interquartile range (IQR), and the box shows the lower and upper intervals of IQR together with the median. We performed pairwise Wilcoxon tests between any two stages to test the significance. The multiple test corrected p-values (Benjamini–Hochberg method) are shown in Table S4; they are all $< 10^{-5}$ except 0-4h vs. 20-24h, for which p-value = 0.26; and 8-12h vs. 16-20h, for which p-value = 0.26.

The gene-level relation between histone modifications and expression variability raises the possibility that the pattern of expression variability across development could be driven by changes in histone modification signal. To compare histone modification signal between stages,

152 we normalized gene and promoter signal by that on intergenic regions (Methods), which are
153 not expected to change histone modification signal between stages. All histone marks present
154 an hourglass-like pattern, with the highest signal at 8-12h (except for H3K4Me1 on gene body,
155 where it is a local but not global maximum), corresponding to E3 and E4, i.e. the lowest
156 expression variability, for both promoters and gene body (Figures 3B-C, S11). Moreover, for
157 all histone marks on gene body, as well as H3K4Me1 on promoters, there is another local
158 maximum at 16-20h, corresponding to E6. Generally, these results support changes in histone
159 modification signal over development, with a correspondence between stronger histone
160 modification signal and lower expression variability.
161
162 Several studies have suggested that mechanisms which confer robustness to stochastic
163 variation can also buffer the effects of genetic variation [7,27,28]. If histone modifications can
164 buffer the effect of genetic variation on gene expression, we should observe that genes with
165 higher histone modification signal are less sensitive to mutations in their regulatory regions,
166 and are thus less conserved. Indeed, genes with higher histone modification signal tend to
167 have less conserved core promoter sequences [29] (49 bp upstream TSS and 10 bp downstream
168 from the TSS) between species (phastCons score; Figure 4A). They are also less conserved
169 within a population (promoter nucleotide diversity π; Figure S12). The phastCons pattern
170 remains using 200 bp or 400 bp regions, but disappears using 1 kb regions (Figure S13),
171 indicating a relatively narrow region around the TSS under this balance of selection and
172 robustness.
173

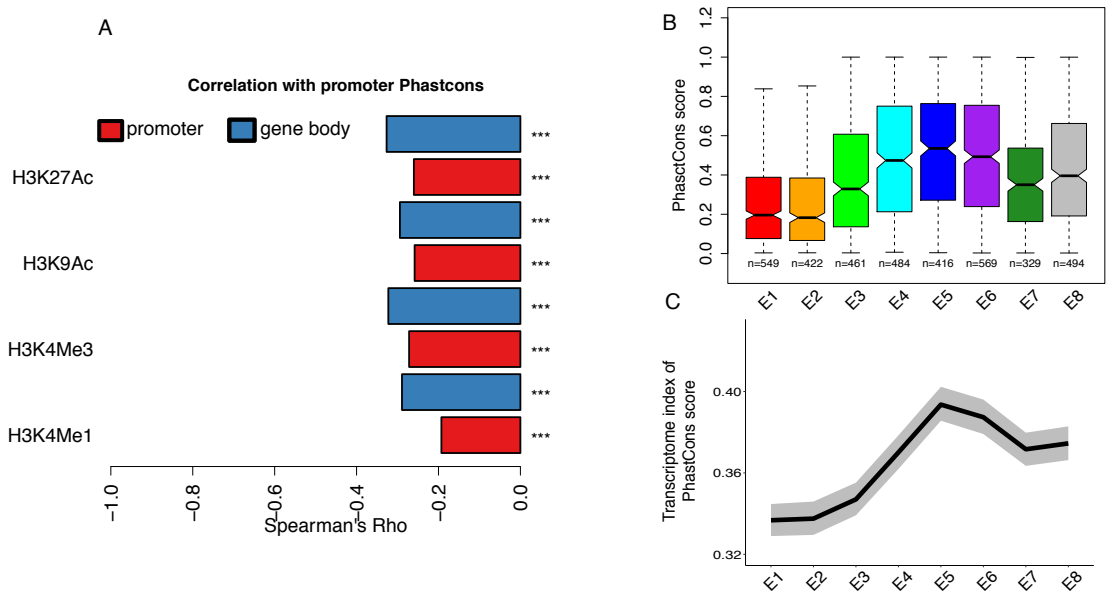

Figure 4: Histone modification signal and promoter sequence conservation

The promoter sequence conservation is the mean of the phastCons score over experimentally identified core promoter regions (49 bp upstream TSS to 10 bp downstream of the TSS) [29].

*A. Spearman's correlation coefficient between histone modification signal (background-subtracted tag density) and promoter sequence conservation. Red and blue represent histone modification signals calculated from the proximal promoter (4 kb around the TSS) and gene body respectively. Here, for each gene, the histone modification signal is the mean value across stages. ***, $P < 0.001$; **, $P < 0.01$; *, $P < 0.05$, NS, $P \geq 0.05$.*

B. Variation of promoter sequence conservation for stage specific genes. The number of genes in each development stage is indicated below each box. We performed pairwise Wilcoxon test between any two stages to test the significance. The multiple test corrected p-values (Benjamini–Hochberg method) are shown in Table S5.

C. Transcriptome index of promoter phastCons score across development. The grey area indicates 95% confidence interval estimated from bootstrap analysis.

Since histone modifications appear to buffer genetic variation in gene expression, and since the E3 stage has stronger modification signals, the lower expression divergence in E3 between species [14] might be caused either by stronger purifying selection on mutations in regulatory regions, or by histone modifications buffering the consequences of mutations in these regions. In the first case, we expect genes specifically expressed at E3 to have higher sequence conservation on promoters. In the second case, we expect the opposite pattern, since mutations that are buffered would behave nearly neutrally. To test this, we identified

genes specifically expressed in each stage and compared their promoter sequence conservation. We found that genes specific of E3 have a relatively weak promoter sequence conservation (Figure 4B), supporting a stronger buffering mechanism rather than stronger purifying selection on sequences. The transcriptome indexes of conservation and of diversity (mean promoter sequence conservation and mean π, respectively, weighted by expression) extend this observation to the full transcriptome (Figure 4C; Figure S14). These results support a role of buffering effects on regulatory mutations in the hourglass pattern of expression divergence in fly embryogenesis.

We have found an uneven distribution of variability, and thus of robustness of the process of gene expression, across development, which mirrors the hourglass Evo-Devo model [9,10]. Stage E3 is the most robust to stochastic variation on gene expression, with lower expression variability, and is the phylotypic stage of fly, with conservation between species [14]. Our results support a role of increased gene and promoter histone modification signal in the lower variability in the phylotypic stage.

Although mutational robustness can evolve under natural selection theoretically [30], the conditions are too restrictive to be relevant in practice. Thus, we propose that the mutational buffering effect of histone modifications is a by-product of selection for minimizing transcriptional noise. The mutational buffering analyses have two potential caveats. First, our results were based solely on promoter analysis, and it remains to be seen how much these observations extend to other regulatory elements. Second, we only considered nucleotide substitution changes, but not insertion, deletion and turnover. For these large effect mutations, purifying selection might be more efficient than mutational robustness to keep conserved expression level. Thus it is possible that both purifying selection and mutational robustness together shape the lower expression divergence in the fly phylotypic stage. Overall, our results support an important role for the control of expression variability by histone modifications in embryonic gene expression and in the evolution of development.

Acknowledgements

We thank Virginie Braman for help with embryo collection and library preparation. We thank Daniel Alpern for help with the BRB-seq technology. We thank Richard Benton, David Garfield and Laurent Keller for critically reading and commenting on the manuscript. We thank Andrea Komljenovic and other members of the Robinson-Rechavi lab for helpful discussions. Part of the computations were performed at the Vital-IT (http://www.vital-it.ch) Center for high-performance computing of the SIB Swiss Institute of Bioinformatics. JL and MRR are supported by Swiss National Science Foundation grants 31003A_153341 / 1 and 31003A_173048. MRR and BD are supported by SystemsX.ch grant AgingX.

Author contributions

JL designed the work with input from MRR, MF and BD. MF led all experiments. JL performed all computational analyses. VG and BD contributed expertise in the BRB-seq experiments. JL and MRR interpreted the results with input from all the other authors. JL wrote the first draft of the paper. JL and MRR finalized the paper with input from all the other authors.

Supplementary figure legends

Figure S1: Relationship between uniquely mapped reads and expressed genes

Each dot represents one sample. The black dots indicate low quality samples with <4500 expressed genes or with <0.3 million uniquely mapped reads. The 239 orange colored samples were retained for downstream analysis ("high quality samples").

Figure S2: Proportion of retained samples in each development stage

The number of retained samples and of total samples in each stage is indicated in the bottom of each bar.

Figure S3: Evidence that the samples from the small cluster are unfertilized eggs

A. Boxplot of Spearman's correlation coefficients (rho) of expression between individual unfertilized eggs and each sample from the small cluster or from the large cluster, showing that the small cluster has an expression profile of unfertilized eggs. The lower and upper intervals indicated by the dashed lines ("whiskers") represent 1.5 times the interquartile range (IQR), and the box shows the lower and upper intervals of IQR together with the median.
B. Expression heat map of meiosis related genes across all samples, showing that their expression decreases over development for the large cluster, but is high in all samples of the small cluster, consistent with unfertilized eggs.

For testing of an alternative explanation of the two clusters as being males and females, see Figure S16.

Figure S4: Relationship between average expression and coefficient of variation at each stage

Pearson's correlation between average expression and coefficient of variation in each development stage is indicated in the top left of each subfigure.

Figure S5: Relationship between average expression and distance to median at each stage

Pearson's correlation between average expression and distance to median in each development stage is indicated in the top left of each subfigure.

Figure S6: Relationship between average expression and adjusted SD at each stage

Pearson's correlation between average expression and adjusted SD in each development stage is indicated in the top left of each subfigure.

Figure S7: Variation of expression variability across development using alternate measures of variability

A. Variability measured by adjusted SD; unlike in Figure 2, the variability in E1 was calculated using all samples from both small and large clusters.
B. Variability measured by coefficient of variation (CV).
C. Variability measured by distance to median (DM).

The legend is the same as for Figure 2. We performed pairwise Wilcoxon test between any two stages to test the significance. The multiple test corrected *p*-values (Benjamini–Hochberg method) are shown in Tables S6, S7 and S8.

Figure S8: Bootstrap analysis of the variability calculation

We performed pairwise Wilcoxon test between any two stages to test the significance. The multiple test corrected *p*-values (Benjamini–Hochberg method) are shown in Table S9.

Figure S9: Variation of expression variability across development for different categories of genes

A. Genes with constant expression level over development.
B. Transcription factor.

The legend is the same as for Figure 2. We performed pairwise Wilcoxon test between any two stages to test the significance. The multiple test corrected *p*-values (Benjamini–Hochberg method) are shown in Tables S10 and S11.

Figure S10: Variation of expression variability across development for dispersed promoter genes and for precise promoter genes

For each stage, the first and the second box represents dispersed promoter genes and precise promoter genes respectively. The legend is the same as for Figure 2. We performed pairwise Wilcoxon test between any two stages to test the significance separately for dispersed promoter genes and for precise promoter genes. The multiple test corrected *p*-values (Benjamini–Hochberg method) are shown in Tables S12 and S13.

306 **Figure S11: Histone modification signal across development**
307 The legend is the same as for Figure 3B and 3C. The median signal value in each
308 development stage is indicated above each box. We performed pairwise Wilcoxon test
309 between any two stages to test the significance. The multiple test corrected *p*-values
310 (Benjamini–Hochberg method) for H3K4Me1, H3K27Ac and H3K9Ac are shown in Tables
311 S14-S19.
312
313 **Figure S12: Spearman's correlation coefficient between histone modification signal**
314 **and promoter nucleotide diversity (π).**
315 The legend is the same as for Figure 4A.
316
317 **Figure S13: Spearman's correlation coefficient between histone modification signal**
318 **and promoter sequence conservation for different definitions of promoter width**
319 The figure legend is the same as in Figure 4A.
320 A. Promoter defined as 200 bp around TSS
321 B. Promoter defined as 400 bp around TSS
322 C. Promoter defined as 1000 bp around TSS
323
324 **Figure S14: transcriptome index of π across development.**
325 The legend is the same as for Figure 4C.
326
327 **Figure S15: Multidimensional scaling analysis for all samples**
328 Different colors indicate different stages. The solid triangles represent high quality samples
329 according to Figure S1; the hollow triangles represent low quality samples which were
330 discarded.
331
332 **Figure S16: Mapping of X/autosome gene expression ratios to the multidimensional**
333 **scaling analysis plot**
334 We calculated the ratio of mean expression between genes from the X chromosome and from
335 the autosomes for each sample. Red represents high ratio, blue represents low ratio. For
336 Drosophila, dosage compensation is achieved by increasing expression of X chromosome
337 genes in males. Since the dosage compensation is still incomplete during development,
338 females should have a higher ratio of mean expression between genes from the X chromosome

339 and from the autosomes. Here, we found both high ratio samples and low ratio samples are
340 well mixed in both the cluster and large clusters. Thus, we reject the hypothesis that the two
341 different clusters are due to sex.
342
343 **Figure S17: Relationship between expression variability and protein importance**
344 We used the average variability across all development stages.
345 A. Spearman's correlation between expression variability and proportion of essential genes.
346 We split genes into 10 equally sized bins based on expression variability. The Spearman's
347 correlation is calculated by using the median variability and proportion of essential genes
348 in the ten bins. The Spearman's correlation coefficient and *p*-value are indicated in the top-
349 right.
350 B. Spearman's correlation between connectivity in a protein-protein interaction network and
351 expression variability. The coefficient and *p*-value are indicated in the top-right.
352
353 **Figure S18: Detection of stage specific genes**
354 A. The artificial expression profile.
355 B. The expression of identified stage specific genes. The bold black line represents the
356 median expression, the two gray lines represent 25th and 75th quantiles of expression,
357 respectively.
358

References

1. Elowitz, M. B., Levine, A. J., Siggia, E. D. & Swain, P. S. Stochastic Gene Expression in a Single Cell. *Science*. **297**, 1183–1186 (2002).
2. Kærn, M., Elston, T. C., Blake, W. J. & Collins, J. J. Stochasticity in gene expression: from theories to phenotypes. *Nat. Rev. Genet.* **6**, 451–464 (2005).
3. Raj, A. & van Oudenaarden, A. Nature, nurture, or chance: stochastic gene expression and its consequences. *Cell* **135**, 216–26 (2008).
4. Raj, A., Rifkin, S. A., Andersen, E. & van Oudenaarden, A. Variability in gene expression underlies incomplete penetrance. *Nature* **463**, 913–8 (2010).
5. Li, X. *et al*. Systems Properties and Spatiotemporal Regulation of Cell Position Variability during Embryogenesis. *Cell Rep*. **26**, 313-321.e7 (2019).
6. Eling, N., Morgan, M. D. & Marioni, J. C. Challenges in measuring and understanding biological noise. doi:10.1038/s41576-019-0130-6
7. Waddington, C. H. Canalization of development and genetic assimilation of acquired characters. *Nature* **150**, 563–565 (1942).
8. Oates, A. C. What's all the noise about developmental stochasticity? *Development* **138**, 601–7 (2011).
9. Raff, R. A. *The shape of life : genes, development, and the evolution of animal form*. (University of Chicago Press., 1996).
10. Duboule, D. Temporal colinearity and the phylotypic progression: a basis for the stability of a vertebrate Bauplan and the evolution of morphologies through heterochrony. *Development* **1994**, 135–142 (1994).
11. Hu, H. *et al*. Constrained vertebrate evolution by pleiotropic genes. *Nat. Ecol. Evol*. **1**, 1722–1730 (2017).
12. Irie, N. & Kuratani, S. Comparative transcriptome analysis reveals vertebrate phylotypic period during organogenesis. *Nat. Commun*. **2**, 248 (2011).
13. Levin, M., Hashimshony, T., Wagner, F. & Yanai, I. Developmental milestones punctuate gene expression in the Caenorhabditis embryo. *Dev. Cell* **22**, 1101–8 (2012).
14. Kalinka, A. T. *et al*. Gene expression divergence recapitulates the developmental hourglass model. *Nature* **468**, 811–4 (2010).
15. Zalts, H. & Yanai, I. Developmental constraints shape the evolution of the nematode mid-developmental transition. *Nat. Ecol. Evol*. **1**, 0113 (2017).
16. Alpern, D. *et al*. BRB-seq: ultra-affordable high-throughput transcriptomics enabled

392 by bulk RNA barcoding and sequencing. *Genome Biol*. **20**, 71 (2019).
393 17. Levin, M. *et al*. The mid-developmental transition and the evolution of animal body
394 plans. *Nature* **531**, 637–41 (2016).
395 18. Schep, A. N. & Adryan, B. A Comparative Analysis of Transcription Factor
396 Expression during Metazoan Embryonic Development. *PLoS One* **8**, e66826 (2013).
397 19. Tadros, W. & Lipshitz, H. D. The maternal-to-zygotic transition: a play in two acts.
398 *Development* **136**, 3033–3042 (2009).
399 20. Schor, I. E. *et al*. Promoter shape varies across populations and affects promoter
400 evolution and expression noise. *Nat. Genet*. **49**, 550–558 (2017).
401 21. Benayoun, B. A. *et al*. H3K4me3 breadth is linked to cell identity and transcriptional
402 consistency. *Cell* **158**, 673–88 (2014).
403 22. Wu, S. *et al*. Independent regulation of gene expression level and noise by histone
404 modifications. *PLOS Comput. Biol*. **13**, e1005585 (2017).
405 23. Nicolas, D., Zoller, B., Suter, D. M. & Naef, F. Modulation of transcriptional burst
406 frequency by histone acetylation. *Proc. Natl. Acad. Sci. U. S. A*. **115**, 7153–7158
407 (2018).
408 24. Weinberger, L. *et al*. Expression Noise and Acetylation Profiles Distinguish HDAC
409 Functions. *Mol. Cell* **47**, 193–202 (2012).
410 25. Faure, A. J., Schmiedel, J. M. & Lehner, B. Systematic Analysis of the Determinants
411 of Gene Expression Noise in Embryonic Stem Cells. *Cell Syst*. **5**, 471-484.e4 (2017).
412 26. Nègre, N. *et al*. A cis-regulatory map of the Drosophila genome. *Nature* **471**, 527–531
413 (2011).
414 27. Lehner, B. Genes Confer Similar Robustness to Environmental, Stochastic, and
415 Genetic Perturbations in Yeast. *PLoS One* **5**, e9035 (2010).
416 28. Meiklejohn, C. D. & Hartl, D. L. A single mode of canalization. *Trends Ecol. Evol*. **17**,
417 468–473 (2002).
418 29. Dreos, R., Ambrosini, G., Périer, R. C. & Bucher, P. The Eukaryotic Promoter
419 Database: expansion of EPDnew and new promoter analysis tools. *Nucleic Acids Res*.
420 **43**, D92–D96 (2015).
421 30. Wagner, G. P., Booth, G. & Bagheri-Chaichian, H. A Population Genetic Theory of
422 Canalization. *Evolution*. **51**, 329 (1997).
423 31. Dobin, A. *et al*. STAR: ultrafast universal RNA-seq aligner. *Bioinformatics* **29**, 15–21
424 (2013).

425 32. Zerbino, D. R. *et al*. Ensembl 2018. *Nucleic Acids Res*. **46**, D754–D761 (2018).
426 33. Anders, S., Pyl, P. T. & Huber, W. HTSeq--a Python framework to work with high-
427 throughput sequencing data. *Bioinformatics* **31**, 166–169 (2015).
428 34. Lun, A. T. L., McCarthy, D. J. & Marioni, J. C. A step-by-step workflow for low-level
429 analysis of single-cell RNA-seq data. *F1000Research* **5**, 2122 (2016).
430 35. Robinson, M. D., McCarthy, D. J. & Smyth, G. K. edgeR: a Bioconductor package for
431 differential expression analysis of digital gene expression data. *Bioinformatics* **26**,
432 139–40 (2010).
433 36. Law, C. W., Chen, Y., Shi, W. & Smyth, G. K. voom: precision weights unlock linear
434 model analysis tools for RNA-seq read counts. *Genome Biol*. **15**, R29 (2014).
435 37. Johnson, W. E., Li, C. & Rabinovic, A. Adjusting batch effects in microarray
436 expression data using empirical Bayes methods. *Biostatistics* **8**, 118–127 (2007).
437 38. Kolodziejczyk, A. A. *et al*. Single Cell RNA-Sequencing of Pluripotent States Unlocks
438 Modular Transcriptional Variation. *Cell Stem Cell* **17**, 471–85 (2015).
439 39. Avilés-Pagán, E. E. & Orr-Weaver, T. L. Activating embryonic development in
440 Drosophila. *Semin. Cell Dev. Biol* ***84****, 100-110* (2018).
441 40. Raser, J. M. & O'Shea, E. K. Noise in gene expression: origins, consequences, and
442 control. *Science* **309**, 2010–3 (2005).
443 41. Tung, P.-Y. *et al*. Batch effects and the effective design of single-cell gene expression
444 studies. *Sci. Rep*. **7**, 39921 (2017).
445 42. Newman, J. R. S. *et al*. Single-cell proteomic analysis of S. cerevisiae reveals the
446 architecture of biological noise. *Nature* **441**, 840–846 (2006).
447 43. Barroso, G. V., Puzovic, N. & Dutheil, J. Y. The Evolution of Gene-Specific
448 Transcriptional Noise Is Driven by Selection at the Pathway Level. *Genetics* **208**, 173–
449 189 (2018).
450 44. Lehner, B. Selection to minimise noise in living systems and its implications for the
451 evolution of gene expression. *Mol. Syst. Biol*. **4**, 170 (2008).
452 45. Quinlan, A. R. & Hall, I. M. BEDTools: a flexible suite of utilities for comparing
453 genomic features. *Bioinformatics* **26**, 841–2 (2010).
454 46. Liu, J. & Robinson-Rechavi, M. Adaptive Evolution of Animal Proteins over
455 Development: Support for the Darwin Selection Opportunity Hypothesis of Evo-Devo.
456 *Mol. Biol. Evol*. **35**, 2862–2872 (2018).
457 47. Alexa, A., Rahnenfuhrer, J. & Lengauer, T. Improved scoring of functional groups

458 from gene expression data by decorrelating GO graph structure. *Bioinformatics* **22**,
459 1600–1607 (2006).
460 48. Huang, W. *et al*. Natural variation in genome architecture among 205 Drosophila
461 melanogaster Genetic Reference Panel lines. *Genome Res*. **24**, 1193–208 (2014).
462 49. Danecek, P. *et al*. The variant call format and VCFtools. *Bioinformatics* **27**, 2156–8
463 (2011).
464 50. Liu, J. & Robinson-Rechavi, M. Developmental Constraints on Genome Evolution in
465 Four Bilaterian Model Species. *Genome Biol. Evol*. **10**, 2266–2277 (2018).
466 51. Domazet-Loso, T. & Tautz, D. A phylogenetically based transcriptome age index
467 mirrors ontogenetic divergence patterns. *Nature* **468**, 815–818 (2010).
468 52. Carbon, S. *et al*. AmiGO: online access to ontology and annotation data.
469 *Bioinformatics* **25**, 288–9 (2009).
470 53. Paris, M., Villalta, J. E., Eisen, M. B. & Lott, S. E. Sex Bias and Maternal
471 Contribution to Gene Expression Divergence in Drosophila Blastoderm Embryos.
472 *PLoS Genet*. **11**, e1005592 (2015).
473 54. Chen, W.-H., Lu, G., Chen, X., Zhao, X.-M. & Bork, P. OGEE v2: an update of the
474 online gene essentiality database with special focus on differentially essential genes in
475 human cancer cell lines. *Nucleic Acids Res*. **45**, D940–D944 (2017).
476 55. Siepel, A. *et al*. Evolutionarily conserved elements in vertebrate, insect, worm, and
477 yeast genomes. *Genome Res*. **15**, 1034–50 (2005).
478
479

480 # Methods

481 **Availability of code**

482 Data files and analysis scripts are available on GitHub:

483 https://github.com/ljljolinq1010/expression-noise-across-fly-embryogenesis.

484

485 **Availability of data**

486 Expression datasets have been deposited to the Gene Expression Omnibus with accession

487 number GSE128370.

488

489 **Embryo collection and RNA extraction**

490 Fly lines (w^{1118}) were obtained from the Bloomington stock center and reared at room

491 temperature on a standard fly medium with 12 hours light dark cycle. The fly medium we used

492 is composed of: 6.2 g Agar powder (ACROS N. 400400050), 58.8 g Farigel wheat (Westhove

493 N. FMZH1), 58.8 g yeast (Springaline BA10), 100 mL grape juice; 4.9 mL Propionic acid

494 (Sigma N. P1386), 26.5 mL of Methyl 4-hydroxybenzoate (VWR N. ALFAA14289.0) solution

495 (400 g/L) in 95% ethanol, 1 L Water. 100 to 150 flies were transferred to cages, which were

496 sealed to a grape agar plate (1:1 mixture of 6% agar and grape juice). We used 4 separate cages

497 to collect the embryos. The adults were kept overnight on this plate before being transferred to

498 a new plate supplemented with yeast paste. Synchronization of eggs on this plate lasted for 2

499 hours before being swapped with a new plate supplemented with yeast paste. We let the adults

500 lay eggs for 30 min before removing the plate and letting the eggs incubate for the desired time.

501 Eggs were harvested using the following protocol. First a 1:1 bleach (Reactolab 99412) 1x PBS

502 mix was poured on the plate and incubated for 2 min. During this incubation, we used a brush

503 to lightly scrape the surface to mobilize the embryos. We then poured the PBS-bleach mixture

504 through a sieve, washed the plate with 1x PBS, and poured the wash on the same sieve. We

505 washed the sieve several time with 1x PBS until the smell of bleach disappeared. Single

506 embryos were then manually transferred to Eppendorf containing 50 μL beads and 350 μL

507 Trizol (lifetechnologies AM9738). The tubes were homogenized in a Precellys 24 Tissue

508 Homogenizer at 6000 rpm for 30 seconds. Samples were then transferred to liquid nitrogen for

509 flash freezing and stored at –80°C. For RNA extraction, tubes were thawed on ice,

510 supplemented with 350 μL of 100% Ethanol before homogenizing again with the same

511 parameters. We then used the Direct-zol™ RNA Miniprep R2056 Kit, with the following

512 modifications: we did not perform DNAse I treatment, we added another 2 min centrifugation

513 into an empty column after the RNA Wash step, finally elution was performed by adding 8 μL
514 of RNAse-free water to the column, incubation at room temperature for 2 min and then
515 centrifugation for 2 min. RNA was transferred to a low-binding 96 well plate and stored at -
516 80°C.
517
518 **Bulk RNA Barcoding and sequencing (BRB-seq)**
519 The BRB-seq is a technique for multiplexed RNA-seq [16] which is able to provide high-quality
520 3' transcriptomic data at a low cost (e.g. 10-fold lower than Illumina Truseq Stranded mRNA-
521 seq). The data (fastq files) generated from BRB-seq are multiplexed and asymmetrical paired
522 reads. Read R1 contains a 6 bp sample barcode, while read R2 contains the fragment sequence
523 to align to the reference genome.
524 1. Library preparation
525 RNA quantity was assessed using picogreen (Invitrogen P11496). Samples were then grouped
526 according to their concentration in 96-well plates and diluted to a final concentration
527 determined by the lowest sample concentration on the plate. RNA was then used for gene
528 expression profiling using BRB-seq. In short, the BRB-seq protocol starts with oligo-dT
529 barcoding, without TSO for the first-strand synthesis (reverse transcription), performed on each
530 sample separately. Then all samples are pooled together, after which the second-strand is
531 synthesized using DNA PolII Nick translation. The sequencing library is then prepared using
532 cDNA augmented by an in-house produced Tn5 transposase preloaded with the same adapters
533 (Tn5-B/B), and further enriched by limited-cycle PCR with Illumina compatible adapters.
534 Libraries are then size-selected (200 - 1000 bp), profiled using High Sensitivity NGS Fragment
535 Analysis Kit (Advanced Analytical, #DNF-474), and measured using Qubit dsDNA HS Assay
536 Kit (Invitrogen, #Q32851). In total, we generated four libraries. For details of library
537 information, please check Table S20.
538 2. Sequencing
539 Libraries were mixed in equimolar quantities and were then sequenced on an Illumina Hi-Seq
540 2500 with pair-end protocol (read R2 with 101 bp) at the Lausanne Genomic Technologies
541 Facility.
542
543 **RNA-seq analysis**
544 1. Generating expression matrix

545 The fastq files were first demultiplexed by using the "Demultiplex" tool from BRB-seqTools
546 suite (available at https://github.com/DeplanckeLab/BRB-seqTools). Then, we trimmed the
547 polyA sequences of the demultiplexed files by using the "Trim" tool. Next, the STAR aligner
548 [31] was used to map the trimmed reads to the reference genome of fly *Drosophila melanogaster*
549 (BDGP6, Ensembl release 91 [32]). Finally, the read count of each gene was obtained with HTSeq
550 [33].
551 2. Filtering samples and genes
552 Low-quality samples need to be filtered out, since they might bias results of downstream
553 analyses. In order to assess sample quality, we calculated the number of uniquely mapped reads
554 and of expressed genes for each sample [34]. We removed samples with <0.3 million uniquely
555 mapped reads or with <4500 expressed genes (Figure S1). We confirmed that these filtered
556 samples are indeed outliers in a multidimensional scaling analysis (MDS) (Figure S15). Since
557 lowly expressed genes have larger technical error, to minimize the technical noise, we need
558 to remove lowly expressed genes as well. We first calculated counts per million (cpm) with
559 the edgeR package [35] for each gene. Then we removed genes with mean cpm across samples
560 ≤1, as suggested by Lun et al.[34]. Finally, for the remaining genes, we re-transformed their
561 cpm values to the original count values for the downstream normalization analysis. After
562 filtering, we obtained an expression count matrix with 239 samples (Figure S2) and 8004
563 protein coding genes.
564 3. Normalization and batch effect correction
565 Because BRB-Seq retains only the 3′ end of the transcript, we performed sample
566 normalization by using quantile normalization with log transformation in the voom package [36],
567 but without transcript length normalization. To remove potential batch effects across the
568 four libraries, we applied the ComBat function in the sva package [37] to the normalized and
569 log2 transformed expression data. For genes with expression values less than 0 after Combat,
570 or with original expression values equal to 0, we change its values to 0 after Combat
571 correction as suggested by Kolodziejczyk et al [38].
572
573 **Multidimensional scaling analysis (MDS)**
574 A number of factors could be invoked to explain the two groups observed in our
575 multidimensional scaling analysis (MDS) (Figure 1B), but they should also explain that only
576 one group is structured according to developmental time. The obvious hypothesis that they
577 correspond to male and female embryos does not explain that structure, and is also not

578 supported by examining X/autosome gene expression ratios (Figure S16). An alternative
579 hypothesis is that samples in the small cluster are unfertilized eggs. If an egg is not fertilized,
580 after completion of meiosis, development will be arrested [39], but they are visually
581 indistinguishable. This hypothesis is confirmed by at least two lines of evidence, in addition
582 to the lack of developmental time structure. First, for expression correlation, all samples in
583 the small cluster are highly correlated with unfertilized egg, while the correlations in the
584 other samples gradually decrease with development (Figure S3A). Second, all the samples
585 from the small cluster are enriched with meiosis related genes (Figure S3B). Thus we
586 excluded the small cluster for downstream analyses, i.e. we used 150 embryos with an
587 average of 18 individuals per developmental stage.
588
589 **Metrics of expression variability**
590 Expression variability is generally measured by the coefficient of variation (CV) [40]. However,
591 a gene's CV is strongly dependent on its RNA abundance (Figure S4). While this is an inherent
592 property of time-interval counting processes (such as a Poisson process), it makes the
593 comparison of variability between different conditions difficult [38,41]. Distance to median (DM,
594 the distance between the squared CV of a gene and its running median) has been proposed as
595 a variability metric that is independent of expression level [38,41,42]. However, the DM is still
596 strongly negatively correlated with the mean expression level in our data (Figure S5). To avoid
597 this dependency, we developed another variability measure, the adjusted standard deviation
598 (adjusted SD), by calculating the ratio between observed SD and expected SD. Following the
599 same approach as Barroso et al. [43], we performed polynomial regressions to predict the
600 expected SD from mean expression. Since the adjusted SD metric works much better than DM
601 in terms of accounting for the confounding effects of mean expression (Figure S6), we adopted
602 it as a measure of expression variability in our study. As observed in yeast [42,44], we found that
603 essential genes and hubs (proteins in the center of protein-protein interaction network) have
604 lower expression variability than other genes (Figure S17), indicating selection to reduce it.
605 This observation provides a control that we are indeed measuring biologically relevant
606 expression variability.
607 Detailed calculation of expression variability:
608 1. Adjusted SD.
609 For each gene, we computed standard deviation (SD) in each stage and over all stages. Then
610 we fitted a polynomial model to predict the global (across all stages) SD from the global mean

611 expression. We increased the degrees of the model until there was no more significant
612 improvement (tested with ANOVA, $p<0.05$ as a significant improvement). Then, based on this
613 best fitting model, for each gene, we computed its predicted global SD based on its global mean
614 expression. Finally, the adjusted SD of a gene in one stage is this gene's SD in its corresponding
615 stage divided by its predicted global SD. This method is derived from Barroso et al. [43], but
616 computing adjusted SD rather than adjusted variance.
617 2. Distance to median: the distance between the squared coefficient of variation (CV) of a
618 gene and its running median.
619 For each gene, we computed its squared CV in each stage and over all stages. Then, we ordered
620 genes based on their global (across all stages) mean expression. Next, we defined series of
621 sliding windows of 50 genes with 25 genes overlap, starting from lowest global mean
622 expression. Finally, the distance to median of a gene in one stage is the stage specific log10
623 squared CV minus the median of global log10 squared CV in this gene's corresponding
624 window. R code was modified from the DM function of the scran package [34].
625
626 **Bootstrap analysis**
627 For each stage, we randomly sampled the same number of samples. Then, we computed the
628 adjusted SD based on these random samples. We repeated the first two steps 500 times. Each
629 time, we only kept the median of the adjusted SD for each stage. Thus in each stage we obtained
630 500 medians. Finally, we performed a Wilcoxon test to test the significance of the difference
631 between the bootstrapped values of different stages.
632
633 **ChIP-Seq data analysis**
634 1. Histone modification signal datasets
635 The signal data files of four euchromatin histone modification marks (H3K4me1, H3K4me3,
636 H3K9ac, and H3K27ac) at six developmental stages (0-4h, 4-8h, 8-12h, 12-16h. 16-20h, 20-
637 24h) were downloaded from modENCODE [26] (NCBI GEO: GSE16013) (March, 2018). The
638 signal is smoothed, background-subtracted tag density. The signal was precomputed along
639 the genome in 35-bp windows.
640 2. Histone modification signal for promoter and gene body
641 For each gene, as suggested by Nicolas et al. [23], we separately calculated the mean signal
642 of its proximal promoter (2 kb upstream to 2 kb downstream for transcription start site (TSS))
643 and of its gene body (TSS to transcription end site (TES)) by using the bedtools "map"

644 command [45]. The TSS and TES information was retrieved from Ensembl release 91 [32]. For
645 a gene with several TSS and TES, we use its mean coordinates.
646 3. Histone modification signal Z score transformation
647 For each modification mark in each stage, the signal value was transformed into a Z score by
648 subtracting the mean signal across intergenic regions and dividing by the standard deviation
649 signal of the intergenic regions. The intergenic region were defined by removing all proximal
650 promoter regions and gene body regions with the bedtools "subtract" command [45]. Our
651 assumption is that on average such intergenic regions are not the target of active histone
652 modification signal, and thus allow to normalize between libraries. Then, for each gene, we
653 re-calculated the mean signal (Z score) of its proximal promoter (2 kb upstream to 2 kb
654 downstream for transcription start site (TSS)) and of its gene body (TSS to transcription end
655 site (TES)) by using the bedtools "map" command [45].
656
657 **Identification of stage specifically expressed genes**
658 Following the same approach as previously [46], we first defined 8 stage specific expressed
659 artificial expression profile (Figure S18A). Then, for each gene, we performed Pearson's
660 correlation between its real expression and this artificial expression. Finally, for each
661 artificial expression profile, we kept genes with top 10% correlation coefficient as the
662 corresponding stage specifically expressed genes (Figure S18B).
663
664 **Identification of hourglass expression variability genes**
665 Similar to the stage specifically expressed gene identification approach, we correlated each
666 gene's variability profile with the median across all genes. Then, we kept genes with the top
667 10% correlation coefficient as the ones following the global hourglass variability profile.
668
669 **Identification of genes expressed at all stages**
670 For each gene, we calculated the average expression across replicates in each stage. Then,
671 we defined the average expression > 1 as expressed.
672
673 **Identification of genes with constant expression across all stages**
674 For each gene, we first preformed one-way analysis of variance (ANOVA) to compare the
675 means of expression in different stage. Then, we calculated the *q-values* for multiple test

676 correction. Finally, the constantly expressed genes were defined as genes with *q-values* >
677 0.05.
678
679 **Gene ontology (GO) enrichment analysis**
680 We performed GO enrichment analysis for hourglass expression variability genes by using
681 the topGO [47] R package with the "elim" algorithm.
682
683 **Single Nucleotide Polymorphism (SNP) data**
684 The SNP data for 205 *D. melanogaster* inbred lines were downloaded from the Drosophila
685 Genetic Reference Panel (DGRP [48]) (December, 2018).
686
687 **Nucleotide diversity (π) calculation**
688 We calculated nucleotide diversity of promoters with vcftools [49].
689
690 **Transcriptome index analysis**
691 A "transcriptome index" [50,51] is a weighted mean of a feature over all genes, where the
692 weights are the expression levels of the genes at each condition (e.g., developmental stage).
693 The transcriptome index of phastCons was calculated as:

$$TPI_s = \frac{\sum_{i=1}^{n} phastCons_i * e_{is}}{\sum_{i}^{n} e_{is}},$$

694
695 where s is the developmental stage, $phastCons_i$ is the promoter sequence conservation score
696 of gene i, n is the total number of genes, and e_{is} is the expression level (log transformed) of
697 gene i in developmental stage s. For the transcriptome index of nucleotide diversity (π) the
698 same formula is used, replacing $phastCons_i$ by π_i.
699
700 **Meiosis related genes and transcription factors**
701 The Meiosis related genes and transcription factors were downloaded from AmiGO [52] (May,
702 2018).
703
704 **Individual unfertilized eggs RNA-seq data**
705 The normalized and log transformed expression matrix of individual unfertilized eggs was
706 downloaded from NCBI GEO: GSE68062 [53] (May, 2018).

707

708 **Dispersed and precise promoters**

709 The annotation of genes with dispersed or precise promoters was downloaded from Schor et
710 al [20] (June, 2019). Dispersed promoters are often associated with ubiquitously expressed
711 genes, have more dispersed patterns of transcriptional initiation, and do not contain a TATA
712 box. On the contrary, precise promoters are typically associated with restricted tissue-specific
713 expression and with a TATA box, and have a single predominant TSS.

714

715 **Essential gene annotation and protein connectivity datasets**

716 The gene essentiality and protein connectivity datasets were downloaded from OGEE v2 [54]
717 (March, 2018).

718

719 **PhastCons score**

720 The pre-computed sequence conservation score phastCons [55] of fly genome was downloaded
721 from http://hgdownload.soe.ucsc.edu/goldenPath/dm3/phastCons15way/ (February, 2018).
722 Higher value means higher conservation.

723

724 **Experimentally validated core promoters**

725 Experimentally validated transcription start sites (TSSs) were downloaded from the
726 Eukaryotic Promoter Database (EPD) [29] (May, 2018). For a gene with several TSSs, we
727 selected the most representative one (the TSS that has been validated by the largest number
728 of samples). The core promoter region was defined as 49 bp upstream TSS to 10 bp
729 downstream of the TSS [29]. We used EPD defined TSSs here because they are more accurate
730 for defining core promoters, whose function is expected to be related to sequence
731 conservation. Whereas for histone modification signal for promoter and gene body we used
732 Ensembl defined TSSs to be consistent with the source of TES information, and precision
733 was less important in defining broader proximal promoters.

734